Tapered Wave with Dominant Polarization State for All Angles of Incidence

Henning Braunisch, *Student Member, IEEE*, Yan Zhang, *Member, IEEE*, Chi O. Ao, Shih-En Shih, *Member, IEEE*, Y. Eric Yang, *Member, IEEE*, Kung-Hau Ding, *Member, IEEE*, Jin A. Kong, *Fellow, IEEE*, and Leung Tsang, *Fellow, IEEE*

***Abstract*—Typical applications of the method of moments (MoM) to rough surface three-dimensional (3-D) electromagnetic scattering require a truncation of the surface considered and call for a tapered incident wave. It is shown how such a wave can be constructed as a superposition of plane waves, avoiding problems near both normal and grazing incidence and providing clean footprints and clear polarization at all angles of incidence. The proposed special choice of polarization vectors removes an irregularity at the origin of the wavenumber space and leads to a least squared error property of the wave. Issues in the application to 3-D scattering from an object over a rough surface are discussed. Approximate 3-D scalar and vector tapered waves which can be evaluated without resorting to any numerical integrations are derived and important limitations to the accuracy and applicability of these approximations are pointed out.**

***Index Terms*—Method of moments, rough surface scattering, tapered wave.**

I. Introduction

RECENT years have seen major advances in the development of fast method of moments (MoM) solvers for three-dimensional (3-D) scattering of electromagnetic vector waves from rough surfaces [1]–[8]. Efforts are now also being directed toward inclusion of objects situated in the neighborhood of the rough surface [9]–[12]. Since the problem of scattering from an object next to a rough surface is computationally complex, two-dimensional (2-D) investigations are also of importance [13]–[20]. The 3-D case with or without objects is aimed at by the present paper.

The methods employed usually require a truncation of the rough surface because of limited computing resources, which leads to erroneous results due to artificial edge diffraction when ideal plane waves are used to excite the system. The tapered wave concept is based on providing an illumination for the numerical simulation that resembles the plane wave case to be modeled closely at the center of the scattering scenario (including a particular arbitrary polarization), while its intensity becomes negligibly small upon approaching the artificially introduced edges of the rough surface. Thus, unwanted edge effects due to the primary incident wave are avoided and the proper normalization of computed scattering coefficients allows a meaningful comparison with the ideal plane wave case; near-field quantities such as current distributions induced near the center of the tapered wave are also expected to be similar.

Furthermore, the tapered wave should be constructed in such a way that it satisfies the Maxwell equations without any approximation. This helps to increase the confidence in the results obtained from the in general rather complex MoM simulation codes. It should also be possible to substitute it for a plane wave of arbitrary polar and azimuthal angles of incidence without loss of polarization and degradation of tapering.

The above requirements led us to revise and modify the tapered wave found in the open literature, which is based on a superposition of plane waves.

II. Superposition of Plane Waves

Consider a homogeneous, isotropic medium with real wavenumber k and wave impedance η. Then the following superposition of a 2-D spectrum of plane waves is an exact solution to the Maxwell equations and represents a wave incident upon the x–y plane from $z > 0$:

$$\overline{E}_i(\overline{r}) = \int_{-\infty}^{\infty} d\overline{k}_\rho \mathrm{e}^{i(\overline{k}_\rho \cdot \overline{\rho} - k_z z)} \psi\left(\overline{k}_\rho\right) \overline{e}\left(\overline{k}_\rho\right) \tag{1}$$

$$\overline{H}_i(\overline{r}) = \int_{-\infty}^{\infty} d\overline{k}_\rho \mathrm{e}^{i(\overline{k}_\rho \cdot \overline{\rho} - k_z z)} \frac{\psi\left(\overline{k}_\rho\right)}{\eta} \overline{h}\left(\overline{k}_\rho\right) \tag{2}$$

where

$$\overline{r} = \overline{\rho} + \hat{z} z \tag{3}$$

$$\overline{k}_\rho = \hat{x} k_x + \hat{y} k_y \tag{4}$$

and

$$k_z = k_z(k_\rho) = \begin{cases} \sqrt{k^2 - k_\rho^2}\,, & 0 \le k_\rho \le k \\ -i\sqrt{k_\rho^2 - k^2}\,, & k_\rho > k \end{cases}. \tag{5}$$

The spectrum ψ carries the information on the shape of the footprint (defined as the distribution of the magnitude in the x–y plane) of the incident field and also on the direction of incidence. It is assumed to be centered about

$$\overline{k}_{i\rho} = \hat{x} k_{ix} + \hat{y} k_{iy} \tag{6}$$

$$= k \sin\theta_i (\hat{x} \cos\phi_i + \hat{y} \sin\phi_i) \tag{7}$$

Manuscript received June 14, 1999; revised March 30, 2000. This work was supported in part by the Office of Naval Research under Contracts N00014-97-1-0172, N00014-99-1-0175 and N00014-92-5-4098 and by the National Science Foundation under Grant ECS-9615799.

H. Braunisch, Y. Zhang, C. O. Ao, S.-E. Shih, K.-H. Ding, and J. A. Kong are with the Research Laboratory of Electronics, Massachusetts Institute of Technology, Cambridge, MA 02139-4307 USA.

Y. E. Yang is with Rannoch Corporation, Cambridge, MA 02142-1100 USA, on leave from the Massachusetts Institute of Technology, Cambridge, MA 02139 USA.

L. Tsang is with the Department of Electrical Engineering, University of Washington, Seattle, WA 98195-2500 USA.

Publisher Item Identifier S 0018-926X(00)06927-1.

where θ_i and ϕ_i are the polar and azimuthal angles of incidence of the central plane wave and—*pars pro toto*—of the tapered wave. In an application, the central plane wave would coincide with the plane wave, which was replaced by the tapered wave in the numerical simulation. Details about the functional dependence of ψ are given in Section III.

The polarization vectors $\overline{e}$ and $\overline{h}$ are of the general form

$$\overline{e}\left(\overline{k}_\rho\right) = e_h\left(\overline{k}_\rho\right)\hat{h}\left(\overline{k}_\rho\right) + e_v\left(\overline{k}_\rho\right)\hat{v}\left(\overline{k}_\rho\right) \tag{8}$$

and

$$\overline{h}\left(\overline{k}_\rho\right) = e_v\left(\overline{k}_\rho\right)\hat{h}\left(\overline{k}_\rho\right) - e_h\left(\overline{k}_\rho\right)\hat{v}\left(\overline{k}_\rho\right). \tag{9}$$

The notations

$$\hat{h}\left(\overline{k}_\rho\right) = \begin{cases} \hat{x}\sin\phi_i - \hat{y}\cos\phi_i, & k_\rho = 0 \\ \dfrac{1}{k_\rho}(\hat{x}k_y - \hat{y}k_x), & k_\rho > 0 \end{cases} \tag{10}$$

and

$$\hat{v}\left(\overline{k}_\rho\right) = \begin{cases} \hat{x}\cos\phi_i + \hat{y}\sin\phi_i, & k_\rho = 0 \\ \dfrac{k_z}{kk_\rho}(\hat{x}k_x + \hat{y}k_y) + \hat{z}\dfrac{k_\rho}{k}, & k_\rho > 0 \end{cases} \tag{11}$$

are found in similar form in [21] and [22]. The chosen definitions for $k_\rho = 0$ take care of the special case of a normally incident pure plane wave. $k_\rho > k$ corresponds to evanescent waves (Section III) and the horizontal part of $\hat{v}(\overline{k}_\rho)$ is imaginary in this case. It is important to note the discontinuity of $\hat{h}$ and $\hat{v}$ at $\overline{k}_\rho = 0$; both *unit* vectors change sign when crossing the origin along a straight line in the $\overline{k}_\rho$ plane.

The general superposition integrals (1) and (2) were stated similarly in [7] and [23]; however, only normal incidence is considered in what follows there. If e_h and e_v in (8) and (9) are set to constants then (1) and (2) specializes to the tapered wave used in [1], [2], [4], [9], and [8], with a particular spectrum ψ briefly discussed in Section III. Problems with this tapered wave encountered near the grazing incidence (for discussion and references see Section III) and near the normal incidence (Section IV) motivated our formulation of a different kind of tapered wave, especially with respect to the polarization vectors.

III. Amplitude Spectrum

If the polarization vector $\overline{e}$ on the right-hand side of (1) is replaced by a scalar constant then the resulting integral

$$\mathcal{E}_i(\overline{r}) = e_i \int_{-\infty}^{\infty} d\overline{k}_\rho \mathrm{e}^{i(\overline{k}_\rho\cdot\overline{\rho} - k_z z)}\psi\left(\overline{k}_\rho\right) \tag{12}$$

is the plane-wave representation of a scalar wave satisfying the scalar Helmholtz equation and ψ can be identified with the well-known angular spectrum in scalar diffraction theory [24], [25]. Thus, by obtaining ψ via 2-D Fourier transformation and making sure that $\overline{e}$ and $\overline{h}$ vary only moderately over the spatial frequency range, where ψ is not negligible, arbitrary footprints of the vector tapered wave can be approximated. [The mentioned requirement leads to a problem with the tapering in [1], [2], [4], [8], and [9] near normal incidence (Section IV).] The information on the direction of incidence of the tapered wave is included by shifting ψ in the k_x–k_y plane to be centered about $\overline{k}_{i\rho}$. The prescribed footprint itself is fixed with respect to angle of incidence.

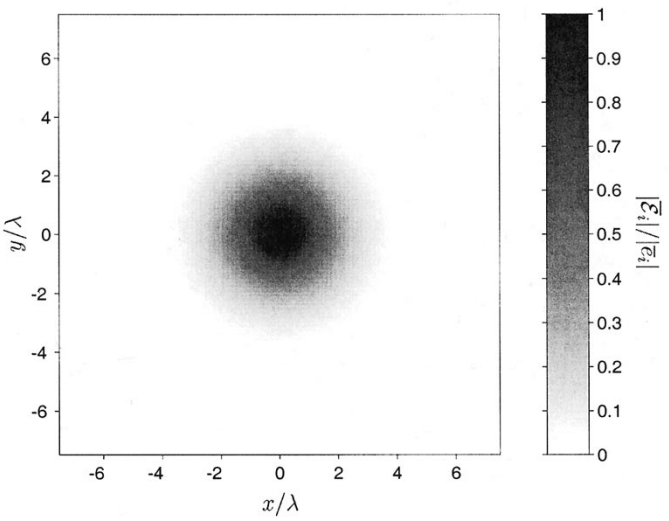

Fig. 1. Example of a prescribed Gaussian-shaped footprint to be approximated by the vector tapered wave ($g = 2\lambda$).

A Gaussian-shaped footprint (Fig. 1) whose amplitude at $\rho = g$ is down to $1/\mathrm{e}$ times the level at the center is implemented by choosing

$$\psi\left(\overline{k}_\rho\right) = \frac{g^2}{4\pi}\,\mathrm{e}^{-g^2|\overline{k}_\rho - \overline{k}_{i\rho}|^2/4}. \tag{13}$$

A pure plane wave is described by $\psi(\overline{k}_\rho) = \delta(\overline{k}_\rho - \overline{k}_{i\rho})$, or $g \to \infty$ in (13). It should be pointed out that, as is well known from signal theory, among all footprints of given finite energy and width, the Gaussian leads to the smallest bandwidth (for the appropriate definition of space- and frequency-domain widths), which is desirable for synthesis.

Spectral components with $k_\rho > k$ are the amplitudes of plane waves that travel along the x–y plane and are evanescent for $z > 0$. Their inclusion makes it possible to synthesize a given footprint near or at grazing incidence.

The spectrum in [1], [2], [4], [8] , and [9] is given as a 2-D Fourier integral that needs to be evaluated numerically. It cannot be used near grazing incidence where the field distribution in the x–y plane becomes highly oscillatory. Its continued use is rooted in its close relation to a scalar tapered wave employed previously [26], [27]. The latter wave, on the other hand, goes back to a popular incident field introduced by Thorsos [28] who, for the 2-D case, derived it as an approximation to a summation of plane waves, accurate for sufficiently *small* angles of incidence θ_i (also employed in [15], [29], [30], and [31]–[33].) The limitations of the 2-D scalar Thorsos wave at low grazing angles were analyzed and discussed in [34] and [35]. The bound in the resolvability criterion discussed by Ngo and Rino [36] also becomes significant at low grazing angles. The recommendation for the 3-D vector case is to start over and simply use the spectrum given by (13), which has the additional benefit of being given in closed form. Taking advantage of the functional dependence of the Gaussian spectrum, an option in the 2-D case is to use path deformation techniques to speed up the evaluation of the exact expression for the incident field [37]. In the 3-D case, we can at least bandlimit the integration to a

disk about $\overline{k}_\rho = \overline{k}_{i\rho}$ within which the spectrum exhibits a significant magnitude (disk radius a few multiples of $2/g$). This leads to an approximation of the original incident field which satisfies Maxwell's equations exactly. The derivation of approximate non-Maxwellian 3-D tapered waves, which can be evaluated without integration is discussed in Section VI.

IV. Polarization

In order to construct a wave that is both reliably tapered and clearly polarized for all angles of incidence, we suggest choosing the polarization of the individual plane wave components as follows:

$$e_h\left(\overline{k}_\rho\right) = \overline{e}_i \cdot \hat{h}\left(\overline{k}_\rho\right) \tag{14}$$

$$e_v\left(\overline{k}_\rho\right) = \overline{e}_i \cdot \hat{v}\left(\overline{k}_\rho\right) \tag{15}$$

with the polarization vector of the central plane wave

$$\overline{e}_i = \overline{e}\left(\overline{k}_{i\rho}\right) = E_h \hat{h}\left(\overline{k}_{i\rho}\right) + E_v \hat{v}\left(\overline{k}_{i\rho}\right). \tag{16}$$

Hence, in dyadic notation

$$\overline{e}\left(\overline{k}_\rho\right) = \overline{e}_i \cdot \left[\hat{h}\left(\overline{k}_\rho\right)\hat{h}\left(\overline{k}_\rho\right) + \hat{v}\left(\overline{k}_\rho\right)\hat{v}\left(\overline{k}_\rho\right)\right] \tag{17}$$

and

$$\overline{h}\left(\overline{k}_\rho\right) = \overline{e}_i \cdot \left[\hat{v}\left(\overline{k}_\rho\right)\hat{h}\left(\overline{k}_\rho\right) - \hat{h}\left(\overline{k}_\rho\right)\hat{v}\left(\overline{k}_\rho\right)\right]. \tag{18}$$

The dominant polarization state of the tapered wave is then determined by the choice of E_h and E_v in (16) which describe the (in general elliptical) polarization of the central plane wave.

Note that with this choice the integrands of (1), (2) are continuous at $\overline{k}_\rho = 0$ [as follows from Section VI, we have, in fact, analyticity throughout the k_x–k_y plane excluding the circle $|\overline{k}_\rho| = k$ provided an analytic spectrum such as (13) is used; at $|\overline{k}_\rho| = k$ the integrands are still continuous] as opposed to the tapered wave in [1], [2], [4], [8], and [9]. The latter wave is characterized by the choice $e_h(\overline{k}_\rho) = E_h$ and $e_v(\overline{k}_\rho) = E_v$, leading to rapidly varying polarization vectors $\overline{e}$ and $\overline{h}$ near $\overline{k}_\rho = 0$. For the near normal incidence case this will violate the basic assumption of the footprint design technique described in Section III. When examined numerically it is found that the approximation of a prescribed, e.g., Gaussian, footprint is poor; the result for normal incidence shows the largest intensity along a ring in the x–y plane rather than at the center (Fig. 2). This effect is also evident from the following consideration: For a spectrum that satisfies $\psi(\overline{k}_\rho) = \psi(-\overline{k}_\rho)$ it can be shown that, for $E_v = 0$, we have $\overline{E}_i(\overline{\rho}, z) = -\overline{E}_i(-\overline{\rho}, z)$ with the consequence $\overline{E}_i(\overline{\rho} = 0, z) = 0$ for all z [Fig. 2(a)]. Similarly, for $E_h = 0$ it is found that $\hat{z} \times \overline{E}_i(\overline{\rho}, z) = -\hat{z} \times \overline{E}_i(-\overline{\rho}, z)$ and $\hat{z} \times \overline{E}_i(\overline{\rho} = 0, z) = 0$ [Fig. 2(b)]. Other problems are leakage of the intensity to larger radii than expected (Fig. 2) and the nonexistence of a clear polarization of the wave. By using (17) and (18) these problems are removed (Fig. 3). [The 101×101 tapered wave field values for the results in Figs. 2, 3, 6, and 7 were calculated using a summation of 128×128 plane waves with a 2-D DFT sampling of the $\overline{k}_\rho$ space. The spectrum after [1], [2], [4], [8], and [9] was calculated using a 2-D FFT algorithm. The horizontal periodicity of the fields in the space domain was in all cases 30 λ, i.e., twice the surface length shown in the figures, in order to avoid aliasing (Section V).]

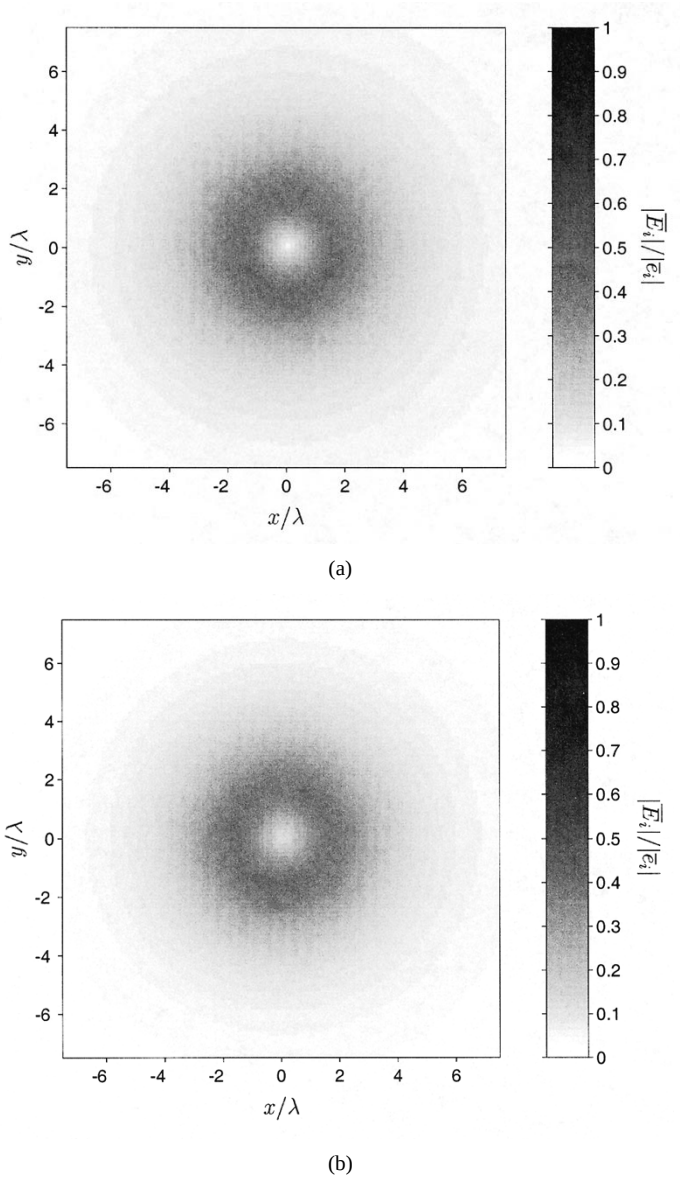

Fig. 2. Resulting footprints at normal incidence for the tapered wave after [1], [2], [4], [8], and [9]. The approximation of the prescribed footprint (Fig. 1) is not satisfactory.

The tapered wave with polarization vectors (17), (18) is optimal in a least squared error sense. Consider a vector field

$$\overline{\mathcal{E}}_i(\overline{r}) = \overline{e}_i \int_{-\infty}^{\infty} d\overline{k}_\rho \mathrm{e}^{i(\overline{k}_\rho \cdot \overline{\rho} - k_z z)} \psi\left(\overline{k}_\rho\right) \tag{19}$$

obtained by multiplying a scalar tapered wave with the constant polarization vector $\overline{e}_i$ as in (16). This field combines the desirable properties of well-defined polarization and controllable tapering. (Note that $|\overline{\mathcal{E}}_i(\overline{\rho}, z = 0)|/|\overline{e}_i|$ corresponds to the prescribed footprint as discussed in Section III and illustrated in Fig. 1.) However, the field defined by (19) is not a valid electric field because in general $\nabla \cdot \overline{\mathcal{E}}_i \neq 0$. We can, therefore, ask for a permissible wave of form (1) with the same spectrum ψ that approximates $\overline{\mathcal{E}}_i$ as close as possible. Defining

$$S(z) = \int_{-\infty}^{\infty} d\overline{\rho} \left|\overline{E}_i(\overline{\rho}, z) - \overline{\mathcal{E}}_i(\overline{\rho}, z)\right|^2 \tag{20}$$

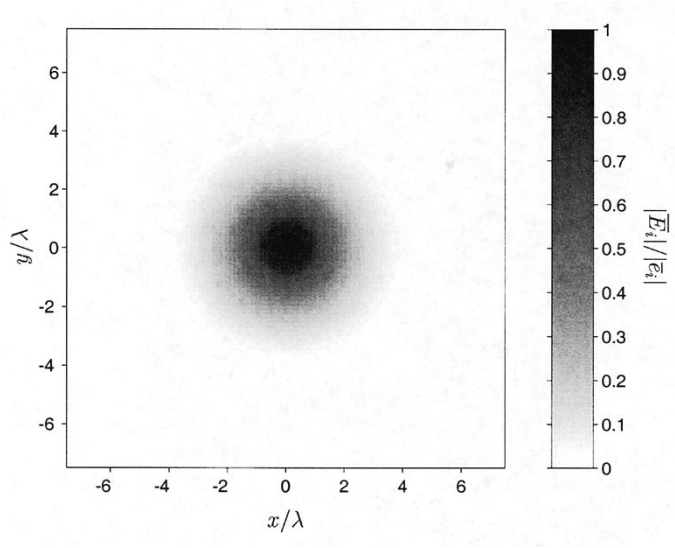

(a)

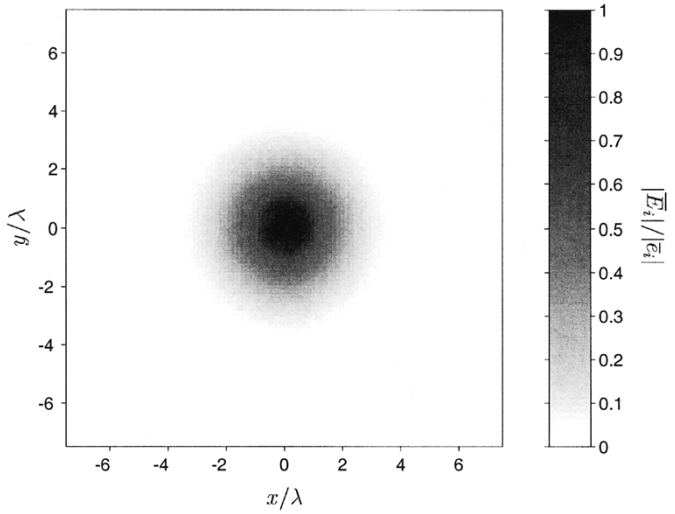

(b)

Fig. 3. Resulting footprints at normal incidence for the tapered wave introduced in the present paper and approximating the prescribed footprint of Fig. 1.

we find from Parseval's theorem for 2-D Fourier transforms

$$S(z) = 4\pi^2 \int_{-\infty}^{\infty} d\overline{k}_\rho \left| \mathrm{e}^{-ik_z z} \psi\left(\overline{k}_\rho\right) \right|^2 \left| \overline{e}\left(\overline{k}_\rho\right) - \overline{e}_i \right|^2. \quad (21)$$

To minimize S for all z, note that

$$\begin{aligned} &\left| \overline{e}\left(\overline{k}_\rho\right) - \overline{e}_i \right|^2 \\ &\quad = \left| \overline{e}\left(\overline{k}_\rho\right) - \overline{e}_i \cdot \left[\hat{h}\left(\overline{k}_\rho\right) \hat{h}\left(\overline{k}_\rho\right) + \hat{v}\left(\overline{k}_\rho\right) \hat{v}\left(\overline{k}_\rho\right) \right] \right|^2 \\ &\qquad + \left| \overline{e}_i \cdot \hat{k}\left(\overline{k}_\rho\right) \right|^2 \end{aligned} \quad (22)$$

where

$$\hat{k}\left(\overline{k}_\rho\right) = \hat{v}\left(\overline{k}_\rho\right) \times \hat{h}\left(\overline{k}_\rho\right) = \frac{1}{k}(\hat{x}k_x + \hat{y}k_y - \hat{z}k_z). \quad (23)$$

Hence, (17) yields the optimal $\overline{E}_i$ and the minimum S_m is given by

$$S_m(z) = 4\pi^2 \int_{-\infty}^{\infty} d\overline{k}_\rho \left| \mathrm{e}^{-ik_z z} \psi\left(\overline{k}_\rho\right) \right|^2 \left| \overline{e}_i \cdot \hat{k}\left(\overline{k}_\rho\right) \right|^2. \quad (24)$$

It is emphasized that we refer to $S(z)$ and $S_m(z)$ as "errors" only in the familiar mathematical sense. The purpose of comparing with the non-Maxwellian field $\overline{\mathcal{E}}_i(\overline{r})$ is to uniquely identify a functional dependence of $\overline{e}(\overline{k}_\rho)$, which can be expected to guarantee tapering and a dominant polarization state of the total field (both as prescribed). In other words, $\overline{\mathcal{E}}_i(\overline{r})$ which is ideal with respect to tapering and polarization is projected into the space of waves constructed as 2-D superpositions of plane waves, lending its desirable properties to an exact solution of Maxwell's equations.

To illustrate the approximation behavior numerically we computed the relative root mean squared (rms) error

$$\sqrt{S(0) \Big/ \int_{-\infty}^{\infty} d\overline{\rho} \left| \overline{\mathcal{E}}_i(\overline{\rho}, 0) \right|^2} = \frac{\sqrt{2S(0)/\pi}}{g|\overline{e}_i|} \quad (25)$$

where $\overline{\mathcal{E}}_i$ is formed using the spectrum (13), for varying tapering parameter g and incidence angle θ_i (in Figs. 4 and 5 contour levels decrease monotonically for fixed θ_i and increasing g and are separated by steps of 2 dB). The results in Fig. 4 for the tapered wave in [1], [2], [4], [8], and [9] exhibit the previously mentioned problems near normal and grazing incidence. It is noted that for intermediate angles θ_i and larger g the error can be smaller than 1% (-20 dB) and that the approximation behavior for horizontally polarized [Fig. 4(a)] and vertically polarized [Fig. 4(b)] plane wave components is similar. For the tapered wave composed according to (17) and (13) and for horizontal polarization [Fig. 5(a)] the error is small everywhere and practically independent of θ_i. For vertical polarization [Fig. 5(b)] the error grows larger toward grazing but does not exceed moderate levels. The fact that approximating a vertically polarized plane wave near grazing incidence is harder can be understood intuitively by noting that the energy flow of the tapered wave has to "bend down" in order to form the exponentially space-limited footprint, a requirement in contradiction with maintaining a vertical polarization state. However, Fig. 5(b) shows that the optimal approximation finds a reasonable compromise. [For the results shown in Figs. 4 and 5, the rms error was evaluated using a Gauss–Legendre quadrature over a surface of size $7g \times 7g$, choosing in both dimensions five times the number of sampling points obtained when rounding $7g/\lambda$ to the nearest integer. 128×128 plane waves were summed to space-domain fields with horizontal periodicity of $7g$. The tapering parameter g was changed in steps of $\lambda/2$ and the angle of incidence θ_i in steps of 5°.]

Another important property of the wave based on (17) is found from (18) by noting that

$$\begin{aligned} \overline{e}_i \cdot \overline{h}\left(\overline{k}_\rho\right) &= \overline{h}\left(\overline{k}_\rho\right) \cdot \overline{e}_i \\ &= \overline{e}_i \cdot \left[\hat{v}\left(\overline{k}_\rho\right) \hat{h}\left(\overline{k}_\rho\right) - \hat{h}\left(\overline{k}_\rho\right) \hat{v}\left(\overline{k}_\rho\right) \right] \cdot \overline{e}_i \\ &= 0 \end{aligned} \quad (26)$$

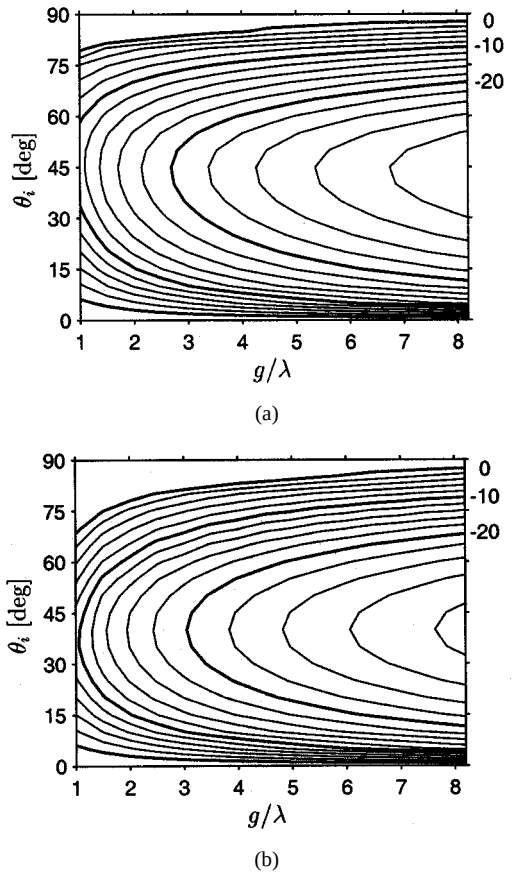

Fig. 4. Relative rms error [dB] at $z = 0$ for the tapered wave after [1], [2], [4], [8], and [9] as compared to a non-Maxwellian field with prescribed tapering and polarization.

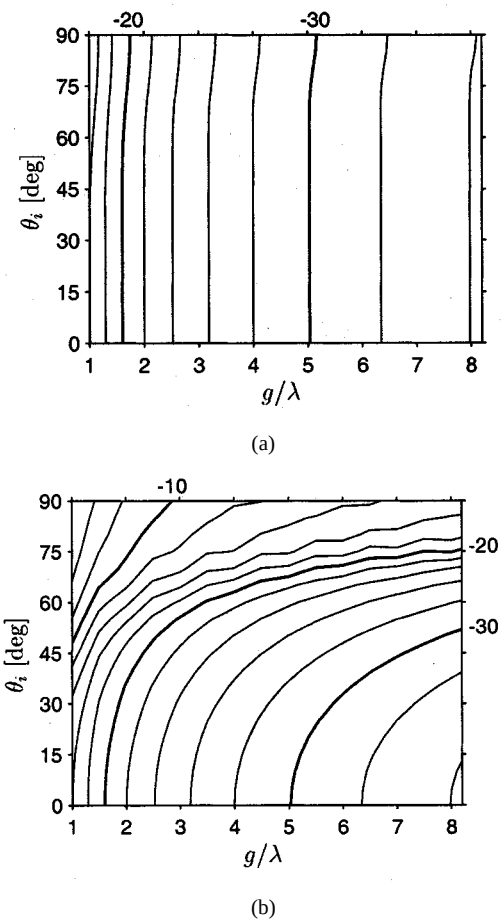

Fig. 5. Relative rms error [dB] at $z = 0$ for the tapered wave introduced in this paper.

and, thus, according to (2), $\overline{e}_i \cdot \overline{H}_i(\overline{r}) = 0$. The total magnetic field of the tapered wave is everywhere perpendicular to the electric field of the central plane wave.

It is remarked that this is reminiscent of the tapered wave (given for the case of normal incidence only) in [23], designed to have no y component of the magnetic field. Setting $\overline{e}_i = -\hat{y}$ in (17), (18) or, more conveniently, in (34) and (37) of Section VI and comparing to (7) and (8) in [23] it is found that the waves are different. In particular, the polarization vectors in [23] are unbounded as $|\overline{k}_\rho| \to k$ while being analytic throughout the k_x-k_y plane excluding the circle $|\overline{k}_\rho| = k$.

The tapered wave given previously by Tran and Maradudin [38] and for the case of vertical polarization employed in [3], [5], and [6]—when generalized to arbitrary azimuthal angle of incidence and cast into our formalism—turns out to be somewhat related. Their magnetic polarization vector for horizontal polarization is collinear to (18) when $E_v = 0$. However, it is normalized to unit length and the magnetic polarization vector for vertical polarization is then obtained by taking the vector product with $\hat{k}(\overline{k}_\rho)$. It is seen that this construction will not lead to an optimal approximation of (19) and, thus, to a different wave.

Finally, we point out that our tapered wave has been derived by optimizing the electric field with respect to an ideal field $\overline{\mathcal{E}}_i$. The magnetic field of the tapered wave then followed from the familiar relation between the electric and magnetic field of a plane wave (Faraday's law). It is clear that in a similar manner we could derive a dual tapered wave which is obtained by choosing the magnetic polarization vectors $\overline{h}$ with respect to a non-Maxwellian field $\overline{\mathcal{H}}_i$ and applying Ampere's law to find the electric field.

V. Issues in the Application to 3-D Scattering

The tapered wave introduced in this paper can be used for the simulation of scattering from randomly rough surfaces with a planar mean surface. In a more complex scenario, objects are embedded in a layered background with rough interfaces. If the objects are at least partially situated in the half space where the sources of the incident wave reside it is important also to pay attention to the distribution of the tapered wave for $z > 0$.

Figs. 6 and 7 illustrate the cases of oblique and grazing incidence, respectively. Fig. 6(a) shows how the tapered wave forms a slightly converging beam, approximating the prescribed footprint at $z = 0$ [Fig. 6(b)]. The nonzero intensity in the top-right corner of Fig. 6(a) is due to the periodic nature of the discretized versions of (1) and (2) with respect to $\overline{\rho}$. This aliasing effect, which in the present case would have no effect on the illumination of objects situated relatively close to the surface at $z = 0$, can be reduced (as usual) by sampling finer with respect to $\overline{k}_\rho$. For footprints where $\psi(\overline{k}_\rho)$ is not given in closed form as in (13), but is computed by 2-D fast Fourier transform (FFT) this is achieved by applying zero padding before carrying out the

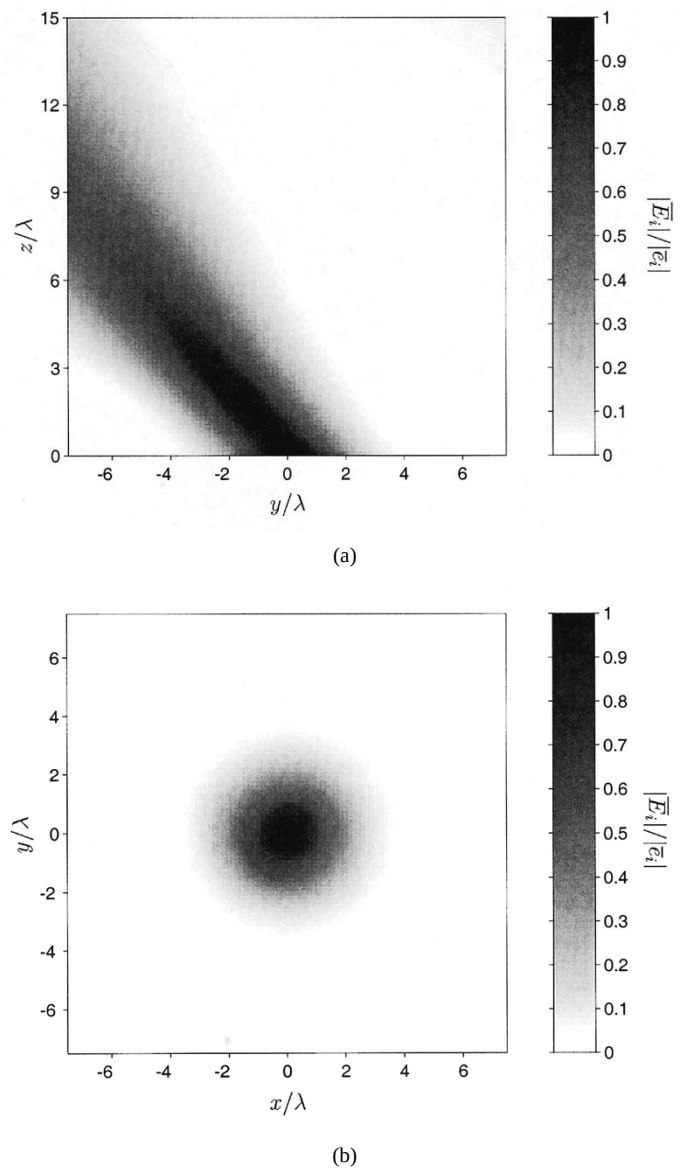

Fig. 6. Beam formation of the tapered wave at oblique incidence ($\theta_i = 40°$, $\phi_i = 90°$, $g = 2\ \lambda$, horizontal polarization).

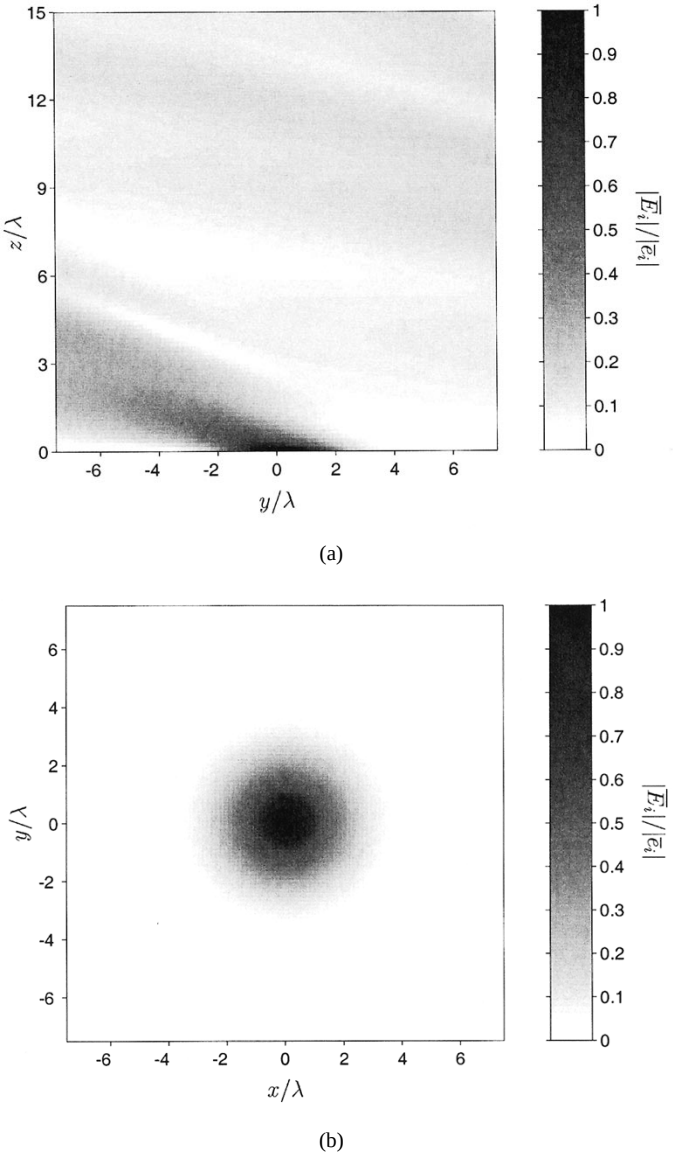

Fig. 7. Beam formation of the tapered wave at grazing incidence ($\theta_i = \phi_i = 90°$, $g = 2\ \lambda$, horizontal polarization).

transformation. The remarkable fact about Fig. 7 is that the inclusion and correct treatment of evanescent waves enables synthesis of the prescribed footprint even for $\theta_i = 90°$ [Fig. 7(b)]. Aliasing for $z > 0$ in this case is more severe [Fig. 7(a)].

In typical applications of the tapered wave concept, electromagnetic wave scattering from a conducting object over a conducting rough surface is simulated and Glisson's overlapping triangular flat vector basis functions [39]–[41] for the electric surface current on both object and rough surface are used in discretizing the electric field integral equation, applying a Galerkin-type method of moments. We compared the results of such a scattering code with those obtained by the hybrid method described in [10]–[12]. The major advantage of this hybrid method is that the decomposition into flat surface problems with impressed equivalent sources that are determined by lower order solutions allows introduction of the tensor Green function for layered media. This removes the need to solve for the surface currents on the rough surface and to truncate its physical dimensions. In the comparison, the same rough surface profile, the same patch model for the object, and the same tapered incident wave were used for solving the problem with the two independent codes; reasonable agreement was obtained. Discrepancies, however, occurred for near-grazing angles $\theta_i = 80° \ldots 90°$ where the pure MoM results suffer from edge effects due to the truncation of the rough surface. While the incident wave can be tapered to fall off exponentially toward the edges the scattered fields from the object decay only as $1/r$, giving rise to problems at very large polar angles where the object acts as a reflector that directs energy toward the edges. This indicates the increased difficulty of the low grazing angle rough surface scattering problem when an object is present. In the hybrid method, the correct behavior of the monostatic horizontal (HH) return at $\theta_i = 90°$ where in the flat surface case the boundary condition on the perfectly conducting surface forces a zero is guaranteed. It should be remarked that although the utilization of the tapered wave concept for the method in [10]–[12], which when

implemented up to and including the first order yields accurate results for slightly rough surfaces, is not imperative, it is still useful there because only finite rough surface profiles can be processed.

VI. Approximate 3-D Tapered Waves

A clear advantage of the original 2-D scalar Thorsos wave and a major reason for its popularity is the avoidance of numerical integrations in the evaluation of the incident field. The price paid is the non-Maxwellian nature of the approximation which, as reported in [34], can lead to anomalies in the computed results of simulations that require evaluation of the incident field not only on the rough surface as, e.g., in object-surface interaction problems. Also the breakdown of the approximation near grazing incidence causes serious problems in some applications. Keeping these limitations in mind and analogous to the derivation of the Thorsos wave, in the 3-D case with the spectrum (13) we can argue, in a spirit similar to Laplace's method for the asymptotic expansion of integrals [42], [43], that for large g the main contribution to the superposition of plane waves comes from around $\overline{k}_\rho = \overline{k}_{i\rho}$. Using the truncated bivariate Taylor expansion in k_x, k_y

$$\begin{aligned}\sqrt{k^2 - \left|\overline{k}_{i\rho} + \overline{k}_\rho\right|^2} &\approx k_{iz} - \frac{k_{ix}}{k_{iz}}\,k_x - \frac{k_{iy}}{k_{iz}}\,k_y \\ &\quad - \frac{k_{ix}k_{iy}}{k_{iz}^3}\,k_xk_y - \frac{k^2 - k_{iy}^2}{2k_{iz}^3}\,k_x^2 - \frac{k^2 - k_{ix}^2}{2k_{iz}^3}\,k_y^2 \end{aligned} \quad (27)$$

where $k_{iz} = k\cos\theta_i$, we can obtain from (12) by carrying out the integrations and symmetrizing the result with respect to x and y (without any further approximations)

$$\mathcal{E}_i(\overline{r}) \approx e_i \mathrm{e}^{i\overline{k}_i\cdot\overline{r}} \frac{1}{u(z)} \exp\left[-\frac{s(\overline{r})}{g^2u^2(z)}\right] \quad (28)$$

where $\overline{k}_i = \overline{k}_{i\rho} - \hat{z}k_{iz}$ and

$$\begin{aligned} s(\overline{r}) &= \left(1 - \frac{2i}{g^2}\,\frac{k^2 - k_{ix}^2}{k_{iz}^3}\,z\right)\left(x + \frac{k_{ix}}{k_{iz}}\,z\right)^2 \\ &\quad + \left(1 - \frac{2i}{g^2}\,\frac{k^2 - k_{iy}^2}{k_{iz}^3}\,z\right)\left(y + \frac{k_{iy}}{k_{iz}}\,z\right)^2 \\ &\quad + \frac{4i}{g^2}\,\frac{k_{ix}k_{iy}}{k_{iz}^3}\,z\left(x + \frac{k_{ix}}{k_{iz}}\,z\right)\left(y + \frac{k_{iy}}{k_{iz}}\,z\right) \end{aligned} \quad (29)$$

and

$$u(z) = \sqrt{\left(1 - \frac{2i}{g^2}\,\frac{k^2}{k_{iz}^3}\,z\right)\left(1 - \frac{2i}{g^2}\,\frac{1}{k_{iz}}\,z\right)}. \quad (30)$$

In deriving (27)–(30), the dispersion relation $k_{iz}^2 = k^2 - k_{ix}^2 - k_{iy}^2$ has been used. As expected, (28) coincides with (12) exactly when $z = 0$. As $g \to \infty$ the plane wave case is recovered. It is remarked that (28) is not a direct generalization of the Thorsos wave to 3-D because of the different formulation of the superposition integral used as starting point. However, using the following argument we arrive at a condition for the validity of (28) that is similar to the one given in the 2-D case [34]–[36], in particular, the dependence on $(\pi/2 - \theta_i)^2$ near grazing carries over to 3-D: The radius of convergence of the full Taylor series (27) is limited to $k - k_{i\rho}$ because of the branch point of the square root function. Thus

$$kg(1 - \sin\theta_i) \gg 1 \quad (31)$$

is required for (28) to be an accurate representation of (12). In addition, the error of the truncated series (27) is multiplied by z with the consequence that the largest $|z|$ considered should be small relative to g, i.e., $g \gg |z|_{\max}$.

Approximations for the 3-D vector wave case are derived in a similar fashion by additionally expanding the polarization vectors. Substituting

$$\hat{h}\left(\overline{k}_\rho\right)\hat{h}\left(\overline{k}_\rho\right) = \frac{1}{k_\rho^2}\left[\hat{x}\hat{x}k_y^2 - (\hat{x}\hat{y} + \hat{y}\hat{x})k_xk_y + \hat{y}\hat{y}k_x^2\right] \quad (32)$$

$$\begin{aligned}\hat{v}\left(\overline{k}_\rho\right)\hat{v}\left(\overline{k}_\rho\right) &= \frac{k_z^2}{k^2k_\rho^2}\left[\hat{x}\hat{x}k_x^2 + (\hat{x}\hat{y} + \hat{y}\hat{x})k_xk_y + \hat{y}\hat{y}k_y^2\right] \\ &\quad + \frac{k_z}{k^2}\left[(\hat{x}\hat{z} + \hat{z}\hat{x})k_x + (\hat{y}\hat{z} + \hat{z}\hat{y})k_y\right] + \hat{z}\hat{z}\frac{k_\rho^2}{k^2}\end{aligned} \quad (33)$$

into (17), we find

$$\begin{aligned}\overline{e}\left(\overline{k}_\rho\right) = \frac{\overline{e}_i}{k^2}\cdot\big[&\hat{x}\hat{x}\left(k^2 - k_x^2\right) + \hat{y}\hat{y}\left(k^2 - k_y^2\right) + \hat{z}\hat{z}k_\rho^2 \\ &- (\hat{x}\hat{y} + \hat{y}\hat{x})k_xk_y + (\hat{x}\hat{z} + \hat{z}\hat{x})k_xk_z \\ &+ (\hat{y}\hat{z} + \hat{z}\hat{y})k_yk_z\big]\,.\end{aligned} \quad (34)$$

Equation (34) also follows from $\hat{h}\hat{h} + \hat{v}\hat{v} = \overline{\overline{I}} - \hat{k}\hat{k}$ with $\overline{\overline{I}}$ the identity tensor and $\hat{k}$ as in (23). Similarly, with the dyads

$$\begin{aligned}\hat{v}\left(\overline{k}_\rho\right)\hat{h}\left(\overline{k}_\rho\right) &= \frac{k_z}{kk_\rho^2}\left[(\hat{x}\hat{x} - \hat{y}\hat{y})k_xk_y - \hat{x}\hat{y}k_x^2 + \hat{y}\hat{x}k_y^2\right] \\ &\quad + \frac{1}{k}(\hat{z}\hat{x}k_y - \hat{z}\hat{y}k_x)\end{aligned} \quad (35)$$

$$\begin{aligned}\hat{h}(\overline{k}_\rho)\hat{v}(\overline{k}_\rho) &= \frac{k_z}{kk_\rho^2}\left[(\hat{x}\hat{x} - \hat{y}\hat{y})k_xk_y + \hat{x}\hat{y}k_y^2 - \hat{y}\hat{x}k_x^2\right] \\ &\quad + \frac{1}{k}(\hat{x}\hat{z}k_y - \hat{y}\hat{z}k_x)\end{aligned} \quad (36)$$

we obtain from (18)

$$\overline{h}\left(\overline{k}_\rho\right) = -\frac{\overline{e}_i}{k}\cdot\left[(\hat{x}\hat{y} - \hat{y}\hat{x})k_z + (\hat{x}\hat{z} - \hat{z}\hat{x})k_y - (\hat{y}\hat{z} - \hat{z}\hat{y})k_x\right]. \quad (37)$$

It is observed from (34) and (37) that the tensors in (17) and (18) are symmetric and anti-symmetric, respectively. More importantly here, it is evident from (34) and (37) that both $\overline{e}(\overline{k}_\rho)$ and $\overline{h}(\overline{k}_\rho)$, viewed as functions of the two real variables k_x and k_y, are analytic throughout the k_x–k_y plane excluding the one-dimensional set of points forming the circle $|\overline{k}_\rho| = k$. (It is emphasized that the region of analyticity includes $\overline{k}_\rho = 0$, c.f. Section IV.) Thus, the Taylor series

$$\overline{e}\left(\overline{k}_{i\rho} + \overline{k}_\rho\right) = \sum_{m,\,n=0}^{\infty} \overline{a}_{mn}k_x^mk_y^n \quad (38)$$

where

$$\overline{a}_{mn} = \frac{1}{m!n!}\left[\frac{\partial^{m+n}}{\partial k_x^m \partial k_y^n}\,\overline{e}\left(\overline{k}_\rho\right)\right]_{\overline{k}_\rho=\overline{k}_{i\rho}} \tag{39}$$

converges in the disk $|\overline{k}_\rho| < k - k_{i\rho}$, and similar expressions hold for $\overline{h}(\overline{k}_\rho)$. Applying the approximation (27) to (1) with the spectrum (13), inserting (38), and using twice the Fourier integral identity (c.f. 3.958.2 in [44])

$$\begin{aligned}\int_{-\infty}^{\infty} dx x^n \mathrm{e}^{iqx-ax^2} &= \sqrt{\frac{\pi}{a}}\, i^{-n}\frac{d^n}{dq^n}\,\mathrm{e}^{-q^2/4a} \\ &= \sqrt{\frac{\pi}{a}}\, n!\left(\frac{i}{2a}\right)^n \mathrm{e}^{-q^2/4a}\sum_{m=0}^{[n/2]}\frac{(-a)^m}{(n-2m)!m!}\,q^{n-2m}\end{aligned} \tag{40}$$

where $[n/2]$ is the integral part of $n/2$, leads, again, without further approximation, to an expression of the form

$$\overline{E}_i(\overline{r}) \approx \mathrm{e}^{i\overline{k}_i\cdot\overline{r}}\frac{1}{u(z)}\exp\left[-\frac{s(\overline{r})}{g^2\,u^2(z)}\right]\sum_{m,\,n=0}^{\infty}\overline{a}_{mn}p_{mn}(\overline{r}) \tag{41}$$

where

$s(\overline{r})$ and $u(z)$	are as in (29) and (30);
the $\overline{a}_{mn}$	are obtained from (34);
$p_{mn}(\overline{r})$	is polynomial in x, y, z up to z-dependent correction factors that, similar to (30), are unity for $z = 0$ or $g \to \infty$.

It is noted that, different from the scalar case discussed above, (41) for $z = 0$ is only an approximation of the superposition of plane waves that we started out with because of the finite radius of convergence of (38) and the fact that the spectrum (13) is not bandlimited. The conditions on g for (41) to be a reasonable approximation are as stated above for the scalar case. We have $\overline{a}_{00} = \overline{e}_i$ and $p_{00} = 1$. Thus, the lowest order electric field approximation following from (41) is the same as what is obtained by approximating k_z in (19) with the help of (27) or multiplying (28) by $\overline{e}_i/e_i$. The p_{mn} of higher order vanish as $g \to \infty$. The algebraic details for the p_{mn} of any order (integrating over k_y first) are as follows:

$$\begin{aligned}p_{mn}(\overline{r}) = n!&\left[\frac{2i}{g^2u_1^2(z)}\right]^n\sum_{k=0}^{[n/2]}\frac{[-g^2u_1^2(z)]^k}{4^k\,k!} \\ &\times\sum_{j=0}^{n-2k}\frac{(m+j)!}{j!(n-2k-j)!}\left(y+\frac{k_{iy}}{k_{iz}}\,z\right)^{n-2k-j} \\ &\times\left(\frac{k_{ix}k_{iy}}{k_{iz}^3}\,z\right)^j\left[\frac{2i}{g^2\,u_2^2(z)}\right]^{m+j} \\ &\sum_{\ell=0}^{[(m+j)/2]}\frac{[-g^2u_2^2(z)]^\ell}{4^\ell(m+j-2\ell)!\ell!} \\ &\times\left[x+\frac{k_{ix}}{k_{iz}}z+w(y,\,z)\right]^{m+j-2\ell}\end{aligned} \tag{42}$$

where

$$u_1^2(z) = 1 - \frac{2i}{g^2}\,\frac{k^2-k_{ix}^2}{k_{iz}^3}\,z \tag{43}$$

$$u_2^2(z) = \frac{u^2(z)}{u_1^2(z)} \tag{44}$$

$$w(y,\,z) = \frac{2i}{g^2\,u_1^2(z)}\,\frac{k_{ix}k_{iy}}{k_{iz}^3}\,z\left(y+\frac{k_{iy}}{k_{iz}}\,z\right). \tag{45}$$

When choosing the number of terms to be included in (41), one should be aware of the limited radius of convergence of (38) and the underlying approximation (27), which, however, has no effect for $z = 0$. The $\overline{a}_{mn}$ with $m + n < 3$ are given by

$$\overline{a}_{00} = \overline{e}_i \tag{46}$$

$$\begin{aligned}\overline{a}_{10} = \frac{\overline{e}_i}{k^2\,k_{iz}}\cdot\big[&-2(\hat{x}\hat{x}-\hat{z}\hat{z})k_{ix}k_{iz}-(\hat{x}\hat{y}+\hat{y}\hat{x})k_{iy}k_{iz} \\ &+(\hat{x}\hat{z}+\hat{z}\hat{x})\left(k_{iz}^2-k_{ix}^2\right) \\ &-(\hat{y}\hat{z}+\hat{z}\hat{y})k_{ix}k_{iy}\big]\end{aligned} \tag{47}$$

$$\begin{aligned}\overline{a}_{01} = \frac{\overline{e}_i}{k^2k_{iz}}\cdot\big[&-2(\hat{y}\hat{y}-\hat{z}\hat{z})k_{iy}k_{iz}-(\hat{x}\hat{y}+\hat{y}\hat{x})k_{ix}k_{iz} \\ &-(\hat{x}\hat{z}+\hat{z}\hat{x})k_{ix}k_{iy}+(\hat{y}\hat{z}+\hat{z}\hat{y}) \\ &\cdot\left(k_{iz}^2-k_{iy}^2\right)\big]\end{aligned} \tag{48}$$

$$\begin{aligned}\overline{a}_{11} = \frac{\overline{e}_i}{k^2k_{iz}^3}\cdot\big[&-(\hat{x}\hat{y}+\hat{y}\hat{x})k_{iz}^3-(\hat{x}\hat{z}+\hat{z}\hat{x})k_{iy}\left(k_{ix}^2+k_{iz}^2\right) \\ &-(\hat{y}\hat{z}+\hat{z}\hat{y})k_{ix}\left(k_{iy}^2+k_{iz}^2\right)\big]\end{aligned} \tag{49}$$

$$\begin{aligned}\overline{a}_{20} = \frac{\overline{e}_i}{2k^2k_{iz}^3}\cdot\big[&-2(\hat{x}\hat{x}-\hat{z}\hat{z})k_{iz}^3-(\hat{x}\hat{z}+\hat{z}\hat{x})k_{ix}(k_{ix}^2+3k_{iz}^2) \\ &-(\hat{y}\hat{z}+\hat{z}\hat{y})k_{iy}\left(k^2-k_{iy}^2\right)\big]\end{aligned} \tag{50}$$

$$\begin{aligned}\overline{a}_{02} = \frac{\overline{e}_i}{2k^2k_{iz}^3}\cdot\big[&-2(\hat{y}\hat{y}-\hat{z}\hat{z})k_{iz}^3-(\hat{x}\hat{z}+\hat{z}\hat{x})k_{ix}\left(k^2-k_{ix}^2\right) \\ &-(\hat{y}\hat{z}+\hat{z}\hat{y})k_{iy}(k_{iy}^2+3k_{iz}^2)\big]\,.\end{aligned} \tag{51}$$

Following a similar procedure, approximations for the magnetic field and the dual tapered wave (Section IV) can be derived.

VII. Conclusion

We considered the problem of constructing a 3-D tapered wave as a superposition of plane waves, taking into account both propagating and evanescent waves. The use of the simple Gaussian plane wave spectrum was recommended in order to avoid problems near the grazing incidence. The introduced special choice for the polarization vectors removed the problems of losing a dominant polarization state and degradation of tapering near the normal incidence. Mathematically speaking, the proposed polarization vectors are analytic at the origin of the 2-D wavenumber space. Moreover, the choice of polarization vectors was shown to lead to an exact solution of the Maxwell equations which is an optimal approximation of an ideal but non-Maxwellian tapered field that is constructed by multiplying a scalar tapered wave with a constant polarization vector. The result is a reliably tapered wave with a dominant polarization state that can be used uniformly for all angles of incidence. We

discussed the application of the proposed tapered wave in simulating 3-D electromagnetic scattering from a conducting object over a conducting rough surface. Newly encountered problems near the grazing incidence were attributed to secondary edge effects that are unrelated to the tapered incident wave, but indicate the difficulty of the low grazing angle rough surface scattering problem when objects are present. It was pointed out that methods which avoid such edge effects could also benefit from the utilization of the tapered wave. In some situations it might be desirable to have an approximate 3-D tapered wave at one's disposal, which does not require a 2-D numerical integration (summation of plane waves), trading accuracy in satisfying Maxwell's equations for computational speed. We presented the derivation of approximations for both the 3-D scalar and vector case. The expansion of the polarization vectors is based on their regularity. The local character of the technique employed forces the breakdown of the approximations at grazing incidence.

REFERENCES

[1] K. Pak, L. Tsang, C. H. Chan, and J. Johnson, "Backscattering enhancement of electromagnetic waves from two-dimensional perfectly conducting random rough surfaces based on Monte Carlo simulations," *J. Opt. Soc. Amer. A*, vol. 12, pp. 2491–2499, Nov. 1995.

[2] J. T. Johnson, L. Tsang, R. T. Shin, K. Pak, C. H. Chan, A. Ishimaru, and Y. Kuga, "Backscattering enhancement of electromagnetic waves from two-dimensional perfectly conducting random rough surfaces: A comparison of Monte Carlo simulations with experimental data," *IEEE Trans. Antennas Propagat.*, vol. 44, pp. 748–756, May 1996.

[3] R. L. Wagner, J. Song, and W. C. Chew, "Monte Carlo simulation of electromagnetic scattering from two-dimensional random rough surfaces," *IEEE Trans. Antennas Propagat.*, vol. 45, pp. 235–245, Feb. 1997.

[4] K. Pak, L. Tsang, and J. Johnson, "Numerical simulations and backscattering enhancement of electromagnetic waves from two-dimensional dielectric random rough surfaces with the sparse-matrix canonical grid method," *J. Opt. Soc. Amer. A*, vol. 14, pp. 1515–1529, July 1997.

[5] V. Jandhyala, E. Michielssen, B. Shanker, and W. C. Chew, "A combined steepest descent-fast multipole algorithm for the fast analysis of three-dimensional scattering by rough surfaces," *IEEE Trans. Geosci. Remote Sensing*, vol. 36, pp. 738–748, May 1998.

[6] ——, "Fast algorithm for the analysis of scattering by dielectric rough surfaces," *J. Opt. Soc. Amer. A*, vol. 15, pp. 1877–1885, July 1998.

[7] J. T. Johnson, R. T. Shin, J. A. Kong, L. Tsang, and K. Pak, "A numerical study of ocean polarimetric thermal emission," *IEEE Trans. Geosci. Remote Sensing*, vol. 37, pp. 8–20, Jan. 1999.

[8] Q. Li, L. Tsang, K. S. Pak, and C. H. Chan, "Bistatic scattering and emissivities of random rough dielectric lossy surfaces with the physics-based two-grid method in conjunction with the sparse-matrix canonical grid method," *IEEE Trans. Antennas Propagat.*, vol. 48, pp. 1–11, Jan. 2000.

[9] G. Zhang and L. Tsang, "Angular correlation function and scattering coefficient of electromagnetic waves scattered by a buried object under a two-dimensional rough surface," *J. Opt. Soc. Amer. A*, vol. 15, pp. 2995–3001, Dec. 1998.

[10] Y. Zhang, "Forward and inverse problems in microwave remote sensing of objects in a complex medium," Ph.D. dissertation, Massachusetts Inst. Technol., Cambridge, MA, 1999.

[11] Y. Zhang, Y. E. Yang, H. Braunisch, and J. A. Kong, "Electromagnetic wave interaction of conducting object with rough surface by hybrid SPM/MoM technique," *J. Electromagn. Waves Applicat.*, vol. 13, pp. 983–984, 1999.

[12] ——, "Electromagnetic wave interaction of conducting object with rough surface by hybrid SPM/MoM technique," in *Progress in Electromagnetics Research (PIER 22)*, J. A. Kong, Ed. Cambridge, MA: EMW, 1999, pp. 315–335.

[13] K. O'Neill, R. Lussky Jr., and K. D. Paulsen, "Scattering from a metallic object embedded near the randomly rough surface of a lossy dielectric," *IEEE Trans. Geosci. Remote Sensing*, vol. 34, pp. 367–376, Mar. 1996.

[14] G. Zhang, L. Tsang, and Y. Kuga, "Studies of the angular correlation function of scattering by random rough surfaces with and without a buried object," *IEEE Trans. Geosci. Remote Sensing*, vol. 35, pp. 444–453, Mar. 1997.

[15] G. Zhang and L. Tsang, "Angular correlation function of wave scattering by a random rough surface and discrete scatterers and its application in the detection of a buried object," *Waves Random Media*, vol. 7, pp. 467–479, July 1997.

[16] A. Madrazo and M. Nieto-Vesperinas, "Scattering of light and other electromagnetic waves from a body buried beneath a highly rough random surface," *J. Opt. Soc. Amer. A*, vol. 14, pp. 1859–1866, Aug. 1997.

[17] J. Ripoll, A. Madrazo, and M. Nieto-Vesperinas, "Scattering of electromagnetic waves from a body over a random rough surface," *Opt. Commun.*, vol. 142, pp. 173–178, Oct. 1997.

[18] A. Madrazo, J. R. Arias-González, and M. Nieto-Vesperinas, "Polarization effects in scattering of electromagnetic waves by an object beneath a random rough surface," *Opt. Commun.*, vol. 162, pp. 91–98, Apr. 1999.

[19] M. Rodríguez Pino, L. Landesa, J. L. Rodríguez, F. Obelleiro, and R. J. Burkholder, "The generalized forward-backward method for analyzing the scattering from targets on ocean-like rough surfaces," *IEEE Trans. Antennas Propagat.*, vol. 47, pp. 961–969, June 1999.

[20] J. R. Arias-González, M. Nieto-Vesperinas, and A. Madrazo, "Morphology-dependent resonances in the scattering of electromagnetic waves from an object buried beneath a plane or a random rough surface," *J. Opt. Soc. Amer. A*, vol. 16, pp. 2928–2934, Dec. 1999.

[21] L. Tsang, J. A. Kong, and R. T. Shin, *Theory of Microwave Remote Sensing*. New York: Wiley, 1985.

[22] J. A. Kong, *Electromagnetic Wave Theory*, 2nd ed. New York: Wiley, 1990.

[23] J. T. Johnson, "Surface currents induced on a dielectric half-space by a Gaussian beam: An extended validation for point matching method of moment codes," *Radio Sci.*, vol. 32, pp. 923–934, May/June 1997.

[24] J. A. Ratcliffe, "Some aspects of diffraction theory and their application to the ionosphere," *Reports Progress Phys.*, vol. 19, pp. 188–267, 1956.

[25] J. W. Goodman, *Introduction to Fourier Optics*. New York: McGraw-Hill, 1968.

[26] L. Tsang, C. H. Chan, and K. Pak, "Monte Carlo simulation of a two-dimensional random rough surface using the sparse-matrix flat-surface iterative approach," *Electron. Lett.*, vol. 29, pp. 1153–1154, June 1993.

[27] ——, "Backscattering enhancement of a two-dimensional random rough surface (three-dimensional scattering) based on Monte Carlo simulations," *J. Opt. Soc. Amer. A*, vol. 11, pp. 711–715, Feb. 1994.

[28] E. I. Thorsos, "The validity of the Kirchhoff approximation for rough surface scattering using a Gaussian roughness spectrum," *J. Acoust. Soc. Amer.*, vol. 83, pp. 78–92, Jan. 1988.

[29] E. I. Thorsos and D. R. Jackson, "Studies of scattering theory using numerical methods," *Waves Random Media*, vol. 1, pp. S165–S190, July 1991.

[30] L. Tsang, C. H. Chan, K. Pak, and H. Sangani, "Monte-Carlo simulations of large-scale problems of random rough surface scattering and applications to grazing incidence with the BMIA/canonical grid method," *IEEE Trans. Antennas Propagat.*, vol. 43, pp. 851–859, Aug. 1995.

[31] D. J. Donohue, H.-C. Ku, and D. R. Thompson, "Application of iterative moment-method solutions to ocean surface radar scattering," *IEEE Trans. Antennas Propagat.*, vol. 46, pp. 121–132, Jan. 1998.

[32] J. T. Johnson, "A numerical study of low-grazing-angle backscatter from ocean-like impedance surfaces with the canonical grid method," *IEEE Trans. Antennas Propagat.*, vol. 46, pp. 114–120, Jan. 1998.

[33] J. V. Toporkov, R. T. Marchand, and G. S. Brown, "On the discretization of the integral equation describing scattering by rough conducting surfaces," *IEEE Trans. Antennas Propagat.*, vol. 46, pp. 150–161, Jan. 1998.

[34] J. V. Toporkov, R. S. Awadallah, and G. S. Brown, "Issues related to the use of a Gaussian-like incident field for low-grazing-angle scattering," *J. Opt. Soc. Amer. A*, vol. 16, pp. 176–187, Jan. 1999.

[35] R. T. Marchand and G. S. Brown, "On the use of finite surfaces in the numerical prediction of rough surface scattering," *IEEE Trans. Antennas Propagat.*, vol. 47, pp. 600–604, Apr. 1999.

[36] H. D. Ngo and C. L. Rino, "Application of beam simulation to scattering at low grazing angles: 1. Methodology and validation," *Radio Sci.*, vol. 29, pp. 1365–1379, Nov./Dec. 1994.

[37] C. H. Chan, L. Tsang, and Q. Li, "Monte Carlo simulations of large-scale one-dimensional random rough-surface scattering at near-grazing incidence: Penetrable case," *IEEE Trans. Antennas Propagat.*, vol. 46, pp. 142–149, Jan. 1998.
[38] P. Tran and A. A. Maradudin, "The scattering of electromagnetic waves from a randomly rough 2D metallic surface," *Opt. Commun.*, vol. 110, pp. 269–273, Aug. 1994.
[39] A. W. Glisson, "On the development of numerical techniques for treating arbitrarily-shaped surfaces," Ph.D. dissertation, Univ. Mississippi, University, MS, 1978.
[40] S. M. Rao, "Electromagnetic scattering and radiation of arbitrarily-shaped surfaces by triangular patch modeling," Ph.D. dissertation, Univ. Mississippi, University, MS, 1980.
[41] S. M. Rao, D. R. Wilton, and A. W. Glisson, "Electromagnetic scattering by surfaces of arbitrary shape," *IEEE Trans. Antennas Propagat.*, vol. AP-30, pp. 409–418, May 1982.
[42] N. Bleistein and R. A. Handelsman, *Asymptotic Expansions of Integrals*. New York: Holt, Rinehart, Winston, 1975.
[43] C. M. Bender and S. A. Orszag, *Advanced Mathematical Methods for Scientists and Engineers*. New York: McGraw-Hill, 1978.
[44] I. S. Gradshteyn and I. M. Ryzhik, *Table of Integrals, Series, and Products*, 5th ed, A. Jeffrey, Ed. New York: Academic, 1994.

Henning Braunisch was born in Hannover, Germany, in 1969. He received the M.S. degree in electrical engineering from Michigan State University, East Lansing, MI, in 1995, and the Dipl. Ing. degree in electrical engineering from the University of Hannover, Germany, in 1996. He is currently working toward the Ph.D. degree at the Department of Electrical Engineering and Computer Science and the Research Laboratory of Electronics, Massachusetts Institute of Technology (MIT), Cambridge.

In 1997, before joining the Center for Electromagnetic Theory and Applications, MIT, he was with Philips Research Laboratories, Hamburg, Germany. He spent the summers of 1995, 1998, 1999, and 2000 at Schlumberger–Doll Research, Ridgefield, CT. His research interests are in applied electromagnetics and acoustics, physics-based signal processing, and forward and inverse modeling.

Dr. Braunisch is an alumnus of the German National Scholarship Foundation (1992–1996), the J. W. Fulbright Foreign Scholarship Board (1994–1995), and the German Academic Exchange Service (1997–1998).

Yan Zhang was born in Sichuan, China in 1963. He received the B.Sc. and M.Sc. degrees in optics from Tsinghua University, Beijing, China, in 1985 and 1987, respectively, the M.A. degree in physics from the City University of New York, NY, in 1993, and the Ph.D. degree in electrical engineering from the Massachusetts Institute of Technology, Cambridge, MA, in 2000.

He is currently working as a Staff Member at the Volpe National Transportation Systems Center of the U.S. Department of Transportation, Cambridge, MA. His research interests are in electromagnetic wave theory, time-domain electromagnetics, wide-band antenna design, and radar signal processing.

Chi O. Ao received the B.A. degree in physics from the University of California at Berkeley, in 1993. He is currently working toward the Ph.D. degree at the Massachusetts Institute of Technology, Cambridge.

His research interests include theoretical and numerical studies of electromagnetic wave scattering in random media and from rough surfaces.

Shih-En Shih received the B.S. and M.S. degrees in electrical engineering from the National Tsing-Hua University, Hsinchu, Taiwan, in 1986 and 1988, respectively, and the Ph.D. degree in electrical engineering from the Massachusetts Institute of Technology, Cambridge, in 1998.

From 1990 to 1991, he was a Product Engineer at Microelectronic Technology Inc., Hsinchu, Taiwan. From 1991 to 1993 he was a Research Engineer at Telecommunication Laboratories, Chung-Li, Taiwan. In 1998 he joined Bell Laboratories, Lucent Technologies, Arlington, VA, where he is an RF System Engineer. His research interests are in RF/microwave circuit design, wave propagation and scattering, microwave remote sensing, and integrated optics.

Y. Eric Yang (M'93) was born in Taichung, Taiwan. He received the Ph.D. degree in electrical engineering from the Massachusetts Institute of Technology (MIT), Cambridge, in 1989.

He was an Electronics Instructor of the Taiwanese Navy from 1981 to 1983. After his Ph.D. studies, he became a Postdoctoral Associate (1989) and then Research Scientist (1990–1999) in the Research Laboratory of Electronics at MIT, where he conducted electromagnetics research in sensors, communications, and navigation applications. He led a multiyear effort to develop EMSARS, a radar image simulation software that combines first-principle electromagnetic scattering theory and a graphical user interface, for several United States Department of Defense programs. He also played a leading role in the MIT/TASC (The Analytic Sciences Corporation) team for the United States Department of Transportation's Microwave Landing System demonstration programs. In addition, he developed computer simulation models for the Civil Aviation Authority of the United Kingdom and the United States Federal Aviation Agency to investigate radio interference to aircraft landing systems and technical issues related to transition from ground-based to satellite-based radionavigation systems. Since December 1999 he has been with Rannoch Corporation, Cambridge, MA, engaged in avionics and aviation systems research and development. His research interest includes the areas of wave propagation in microelectronic circuits, computational techniques, electromagnetic interference in electronic systems, wave propagation, scattering, and radar imaging simulation.

Dr. Yang is a member of the Electromagnetics Academy and Sigma Xi. He received the triennial Henry George Booker Award for Young Scientist by the URSI United States National Committee in 1990.

Kung-Hau Ding (S'85–M'89) received the B.S. degree in physics from the National Tsing-Hua University, Hsinchu, Taiwan, and the M.S. (physics and electrical engineering) and Ph.D. (electrical engineering) degrees from the University of Washington, Seattle.

He is currently a Research Engineer at the Sensors Directorate of the Air Force Research Laboratory, Hanscom Air Force Base, MA. From 1989 to 1993 he worked as a Physical Scientist at the Physical Science Laboratory, New Mexico State University, Las Cruces. From 1993 to 1998 he was a Research Scientist at the Research Laboratory of Electronics, Massachusetts Institute of Technology, Cambridge. His research interests include wave propagation and scattering in random media, microwave remote sensing, and radar clutter and target characterizations.

Dr. Ding is a member of The Electromagnetics Academy.

Jin A. Kong is a Professor of electrical engineering at the Massachusetts Institute of Technology, Cambridge, MA, where he is also the Chairman of Area IV on Energy and Electromagnetic Systems in the Department of Electrical Engineering and Computer Science and Director of the Center for Electromagnetic Theory and Applications in the Research Laboratory of Electronics. He has been principal investigator for more than 100 grants and contracts from various government agencies and industry. He has served as Consultant, External Examiner, and Advisor to industry, academia, national governments, and the United Nations. He has been Reviewer for many journals, book companies, and government agencies. He has published over 20 books including *Electromagnetic Wave Theory* (New York: Wiley, 1975, 1986, 1990; Cambridge, MA: EMW, 1998), over 200 refereed journal articles and book chapters, over 300 conference papers, and supervised over 150 theses. He is editor for the *Wiley Series in Remote Sensing*, editor-in-chief for the *Journal of Electromagnetic Waves and Applications (JEMWA)*, and chief editor for the book series *Progress In Electromagnetics Research (PIER)*. His research interest is in the area of electromagnetic wave theory and applications.

Prof. Kong has served as session chairman, organizer, member of the technical program committees for numerous international and national conferences and symposia, including serving as chairman for the *Progress In Electromagnetics Research Symposium (PIERS)* since 1989. He is the recipient of the S. T. Li Prize for the year 2000. He is the President of The Electromagnetics Academy.

Leung Tsang (S'73–M'75–SM'85–F'90) received the B.S. degree in 1971, the M.S. and E.E. degrees in 1973, and the Ph.D. degree in 1976, all from the Massachusetts Institute of Technology, Cambridge.

He has been a Professor of Electrical Engineering, University of Washington, Seattle, since 1986. He is a coauthor of *Theory of Microwave Remote Sensing* (New York: Wiley, 1985). His current research interests are in remote sensing, wave scattering and propagation in random media, and optoelectronics.

Dr. Tsang was the Technical Program Chairman of the 1994 IEEE Antennas and Propagation International Symposium and also the Technical Program Chairman of the 1995 Progress in Electromagnetics Research Symposium (PIERS). He was General Chairman of IGARSS 1998. Since 1996 he has been editor of the IEEE TRANSACTIONS ON GEOSCIENCE AND REMOTE SENSING. He is a Fellow of the Optical Society of America.